ResearchGate

See discussions, stats, and author profiles for this publication at: https://www.researchgate.net/publication/240764141

Position-selective growth of carbon nanotubes on Ni catalysts/Mo underlayers by thermal chemical vapor deposition

Article *in* Journal of Materials Research · November 2006

DOI: 10.1557/jmr.2006.0351

CITATIONS
2

READS
1,358

3 authors, including:

Nobuyuki Iwata
Nihon University
103 PUBLICATIONS **653** CITATIONS

SEE PROFILE

Hiroshi Yamamoto
Nihon University
117 PUBLICATIONS **436** CITATIONS

SEE PROFILE

All content following this page was uploaded by Hiroshi Yamamoto on 14 June 2016.

The user has requested enhancement of the downloaded file.

Petitioner Runergy USA Inc., Ex. 1033, p. Cover

Position-selective growth of carbon nanotubes on Ni catalysts/Mo underlayers by thermal chemical vapor deposition

Hiroki Okuyama,[a] Nobuyuki Iwata, and Hiroshi Yamamoto
College of Science and Technology, Nihon University, Funabashi, Chiba 274-8501, Japan

(Received 3 April 2006; accepted 12 July 2006)

Position-selective growth of carbon nanotubes (CNTs) and vertically aligned CNTs (VACNTs) on patterned metal were prepared using thermal chemical vapor deposition (TCVD) and direct current (DC) plasma-enhanced chemical vapor deposition. We propose a new position-controlling method of CNTs by controlling not only the position of Ni as a catalyst, but also the morphology of Mo as an underlayer for the catalysts. Selective growth of CNTs was achieved at the edges of the patterned metal using TCVD. The minimum width of selectively grown CNTs, approximately 2.6 μm, was approximately one-eightieth that of the patterned metal, 200 μm. The VACNTs were synthesized using the PECVD method, but the VACNTs grew throughout the patterned metal. A position-controlled method of CNT growth was demonstrated in optimum conditions of the TCVD.

I. INTRODUCTION

Carbon nanotubes (CNTs) have been studied intensively because of their many featured characteristics such as high electric conductivity,[1] high permissible current density,[2] and high mechanical strength in spite of their high flexibility.[3] These characteristics are beneficial in preparing various nanostructures for use in scanning-probe microscopy tips,[4–6] field emitters,[7–9] and so on. To prepare such nanoscaled CNT devices, the controlling position and direction of CNTs is necessary. CNTs grow selectively from catalyst particles using chemical vapor deposition (CVD).[10] The growth direction of CNTs is controlled by applying an electric field during CVD growth.[11]

Position-selective growth of CNTs is possible by virtue of two characteristics: CNTs grow selectively from fine particle catalysts, and, we can control the synthesis of the fine particle catalysts by noticing wettability between metal interfaces. Wettability of metal interface is high. Therefore, it is difficult to form fine particles as overlayers on smooth underlayers. Overlayered metals form fine particles when the surfaces of underlayers are rough. In this article, we propose a new position-controlled method of CNT growth by controlling not only the catalysts' position, but also surface morphology of metal underlayers. We tried to prepare position-selective growth of CNTs and vertically aligned CNTs (VACNTs) on patterned metal electrodes to realize a novel electronic measuring nanoprobe.

II. EXPERIMENTAL

Patterned metals of Ni catalysts and Mo underlayers were deposited on quartz substrates through a metal mask (thickness of 30 μm, pattern width of 200 μm, and gap of 100 μm) using radio frequency (RF) magnetron sputtering. The chamber background pressure was 3.0×10^{-3} Pa, and the pressure during deposition was fixed at 2.0 Pa by feeding Ar gas. Growth conditions were 120 °C of substrate temperature, 50 W of sputtering power, and 1 min of sputtering time for Mo underlayers, and 70 °C, 20 W, and 1 min for Ni catalysts. The films' deposition rates were 10 nm/min^{-1} for Mo and 1 nm/min^{-1} for Ni. To control incident angles of sputtered atoms, aligned fins were installed during deposition. A schematic configuration of the fins and the metal mask is shown in Fig. 1.

The CNTs were grown using thermal chemical vapor deposition (TCVD) and direct current (DC) plasma-enhanced (PE) CVD methods. The CVD equipment reactor tube was heated to 600 °C. The background pressure was 0.1 Pa. The flow of H_2:Ar (10:200 ccm) was introduced into the reactor tube during heating. In the case of a TCVD method, a gas mixture of ethylene C_2H_4:H_2:Ar (20:10:200 ccm) was introduced into the reactor tube for 30 min for CNT growth. The total pressure was maintained at 100 kPa. In the case of the PECVD method, the CNT growth was performed by inducing a

[a] Address all correspondence to this author.
e-mail: okuyama@yamanoya.ecs.cst.nihon-u.ac.jp
DOI: 10.1557/JMR.2006.0351

 © 2006 Materials Research Society

Petitioner Runergy USA Inc., Ex. 1033, p. 2888

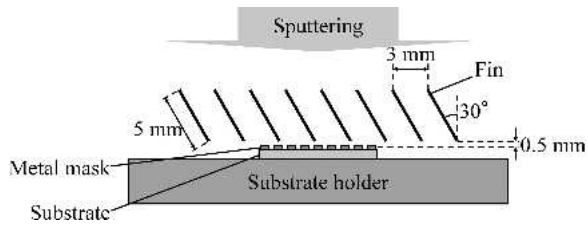

FIG. 1. Schematic configuration of the fins and the metal mask.

DC glow discharge and feeding a gas mixture of C_2H_4:H_2:Ar (5:50:50 ccm). The total pressure was maintained at 2 kPa. The DC plasma was produced by applying a bias voltage of −250 V between a substrate holder and grounded anodes, which were separated from the substrates by approximately 5 mm.

The patterned metals' respective morphologies were investigated using atomic force microscopy (AFM, NanoNavi Station; SII Nanotechnology, Inc., Tokyo, Japan). The CNTs' structures were observed using a field emission scanning electron microscope (SEM; S-4500; Hitachi Ltd., Tokyo, Japan) operated at 15 kV and a field emission transmission electron microscope (TEM; HF-2000; Hitachi Ltd.) operated at 200 kV.

III. RESULTS AND DISCUSSION

Figure 2 shows AFM images (5×5 μm^2) of the patterned metal layers immediately before CNT growth. Figures 2(a) and 2(b), respectively, show the edge boundary of patterned metal layers and the middle areas of the patterned metal. Figure 2(c) shows scanned areas of Figs. 2(a) and 2(b). The left of Fig. 2(a) shows the substrate surfaces; the right shows the patterned metal layers. At the pattern edges, large Ni particles with an approximate 30-nm height were observed on small Mo particles with an approximate 3-nm height. At the middle areas of the pattern [Fig. 2(b)], only a few particles were observed on smooth surfaces. Figure 3 shows SEM images of the edge boundary of the patterned metal layers after TCVD deposition at varying thickness of the Mo

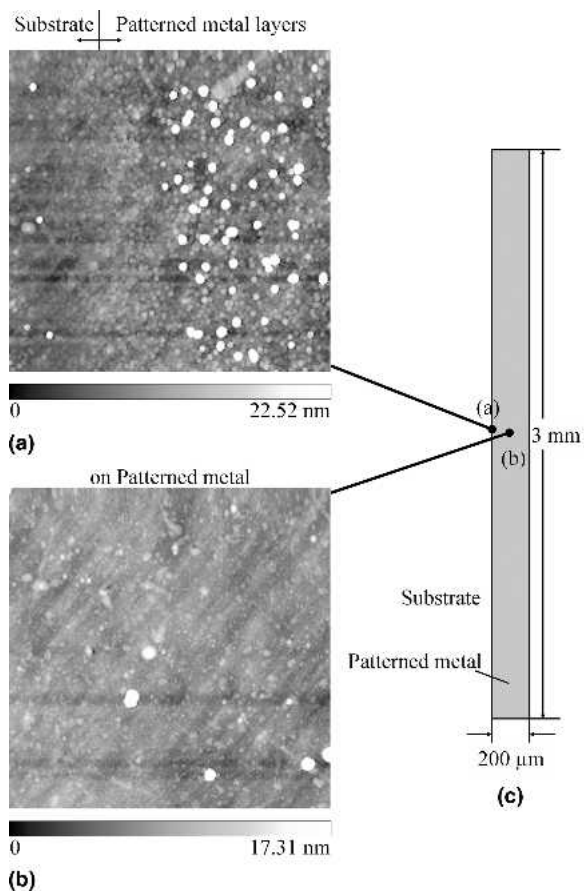

FIG. 2. (a) and (b) AFM images (5×5 μm^2) of patterned metal layers. (c) The scanning area of the AFM images. (a) The edge boundary of patterned metal layers. The left of the AFM image shows the substrate surfaces; the right shows the patterned metal layers. (b) The middle areas of the patterned metal.

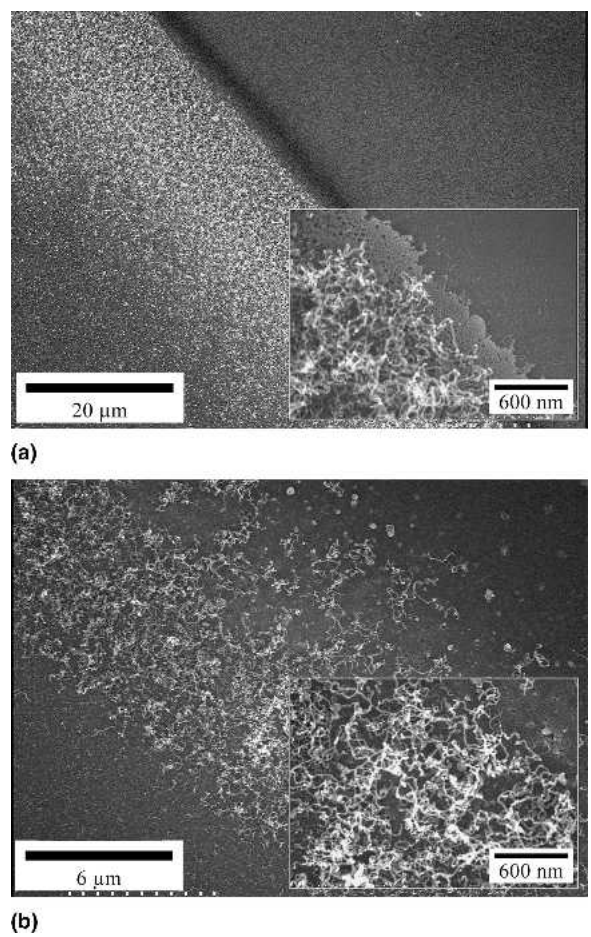

FIG. 3. SEM images of patterned metal layer boundary edges after TCVD while varying the Mo underlayer thickness. The Mo layers were (a) 10 nm and (b) 30 nm thick. The upper-right of the image shows the substrate surfaces; the lower-left shows the patterned metal layers. The CNTs grew in the narrow region that appears as the white contrast. The W_{CNT} was approximately (a) 30 μm and (b) 6.3 μm. The insets are magnified images.

Petitioner Runergy USA Inc., Ex. 1033, p. 2889

underlayer. Thickness of the Mo layers was 10 nm [Fig. 3(a)] and 30 nm [Fig. 3(b)]. The upper-right of the image shows the substrate surfaces; the lower-left shows the patterned metal layers. The CNTs, with an approximate 30-nm diameter, grew selectively immediately inside from the pattern edges that appear in the image as the white contrast. However, CNTs did not grow on the middle areas of the pattern. By increasing the Mo thickness from 10 nm [Fig. 3(a)] to 30 nm [Fig. 3(b)], the widths of selectively grown CNTs (W_{CNT}) decreased respectively from 30 μm [Fig. 3(a)] to 6.3 μm [Fig. 3(b)]. The CNT diameter was similar to that of the Ni particle, as observed using AFM. At the pattern edges, many small Mo particles were observed under the CNTs.

The position-selective growth of CNTs at the pattern edges was achieved because CNTs grow only from fine particle catalysts. Delzeit et al.[12] reported that no CNT was grown with 0.1–1.0 nm Fe on smooth, clean Si substrates. The CNTs grew by the addition of an Ir underlayer to increase the surface roughness and to provide more active nucleation sites. On the smooth surface of Mo underlayers, it is difficult for Ni catalysts to become fine particles because of the high wettability. The rough morphology of Mo underlayers provides active nucleation sites for Ni catalysts. The rough morphology was apparent in very thin regions of Mo because of a "shadow effect" of the sputtering method. A schematic shadow effect is illustrated in Fig. 4. Sputtered atoms arrive at substrates with various incident angles because of scattering by atmospheric gasses. Then the pattern edges thin down by deposition of particles shaded from the mask pattern. The rough regions of thicker Mo underlayers became narrow. Therefore, the W_{CNT} decreased by increasing Mo thickness.

Figure 5 shows SEM images of the pattern boundary after TCVD at varying sputtering pressures of metal layers. The W_{CNT} was decreased from 230 to 6.4 μm by reducing sputtering pressure from 4.0 to 1.2 Pa.

The shady region by metal mask is decreased by reducing sputtering pressure because incident angle variations of sputtered atoms are decreased. Therefore, by reducing sputtering pressure, the metal pattern edge was sharpened and W_{CNT} was reduced.

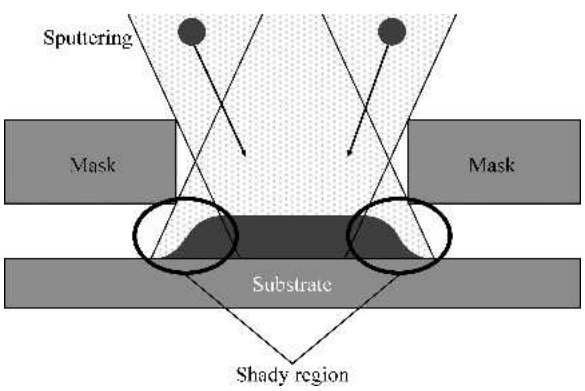

FIG. 4. Schematic of the "shadow effect" that appeared through the mask pattern. The pattern edges thin down because of deposition of shaded sputtered atoms under the mask edges (indicated by the oval).

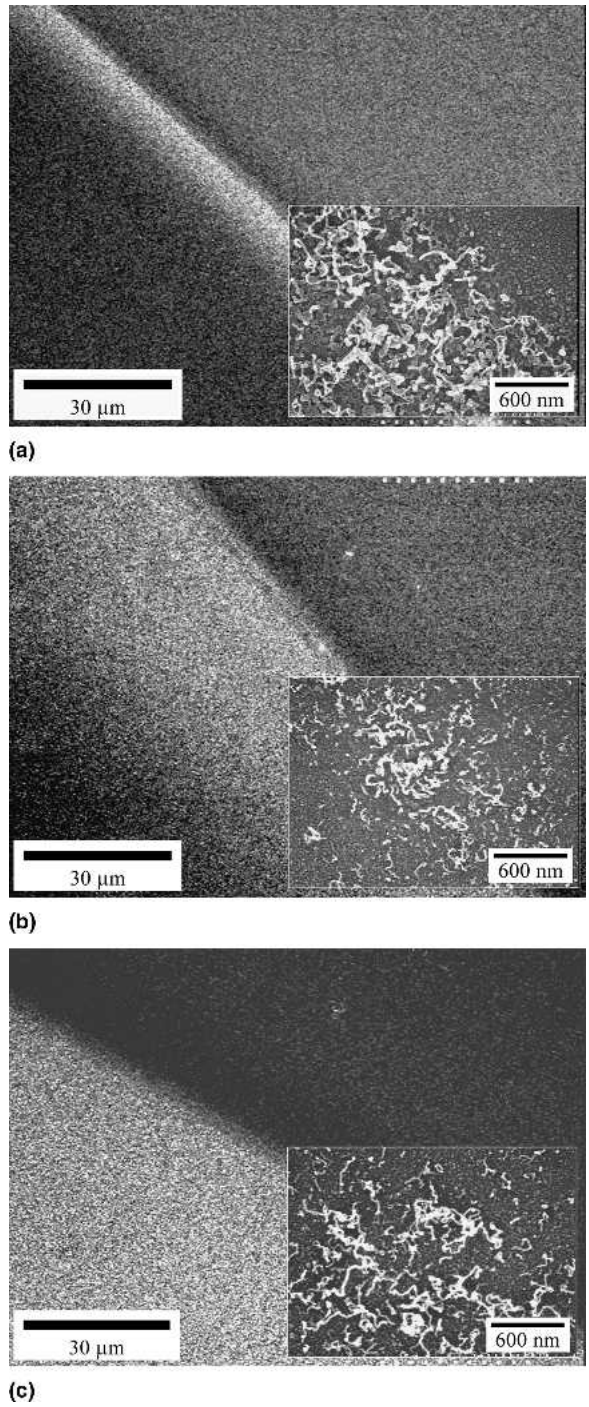

FIG. 5. SEM images of the edge boundary of patterned metal layers after TCVD at varying sputtering pressure of metal layers. The sputtering pressure of the metal layers was (a) 1.2 Pa, (b) 2.0 Pa, and (c) 4.0 Pa. The upper-right at the image is the substrate, the lower-left of the image is the metal pattern. The CNTs grew at narrow region where the contrast of the SEM image is white. The W_{CNT} was (a) 6.4 μm, (b) 26 μm, and (c) 230 μm. The inset shows magnified images.

Petitioner Runergy USA Inc., Ex. 1033, p. 2890

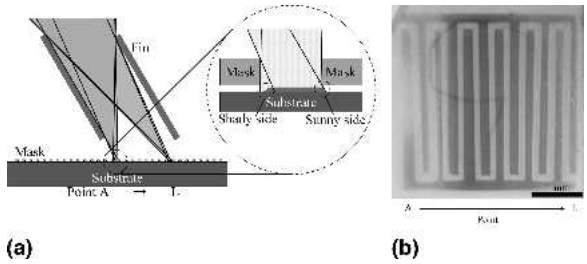

FIG. 6. (a) Schematic configuration of the aligned fins and the mask. (b) An optical microscopy image of a specimen prepared by installing the fins.

The aligned fins were installed during deposition to control incident angles of sputtered atoms. A schematic configuration of the fins and the metal mask is depicted in Fig. 6(a). The optical microscopy image of the patterned metal, which was sputtered through the fins, is shown in Fig. 6(b). The pattern contrast was not uniform because the metal pattern thickness was not uniform. For that reason, various metal pattern thicknesses can be evaluated simultaneously on this sample. Figure 7 shows typical SEM images of the pattern boundary after TCVD by installing the fins during Mo deposition. Figures 7(a) and 7(b), respectively, show the results on the edges of point D, and Figs. 7(c) and 7(d) show the results on the edges of point K. The images in Figs. 7(a) and 7(c) depict the "shady side"; the upper-right of the image shows the metal pattern. Images in Figs. 7(b) and 7(d) portray the "sunny side"; the lower-left of the image shows the metal pattern. The CNTs grew in the narrow region that appears as the white contrast. The W_{CNT} was (a) 17 μm, (b) 2.6 μm, (c) 29 μm, and (d) 19 μm. The W_{CNT} for every pattern is summarized in Fig. 8. The gray belts correspond to metal mask patterns and white belts correspond to the pattern gaps. The results show that the W_{CNT} was narrower on the "sunny side" than on the "shady side." In addition, the W_{CNT} depended on the position of the pattern. The minimum W_{CNT} was 2.6 μm. This width was approximately one-eightieth of the pattern width.

At pressures of 2.0 Pa, the sputtering condition of the mean free path of sputtered atoms was approximately 6 mm, which was slightly longer than the fin length of 5 mm. The sputtered atoms travel straight through vacancies of the fins. The incident angles of sputtered atoms were limited by the fins. The incident angle distributions were calculated. The width between the maximum and the minimum distance of the shaded area was determined as an effective width considering the shadow effect (W_{SE}). The solid lines in Fig. 8 show the W_{SE}. The gap between the mask and the substrate was fixed as about 5 μm. In calculation results, the W_{SE} was uniform between Points C and I. The respective W_{SE} of sunny and shady sides were 3 and 22 μm. The W_{SE} and W_{CNT} of

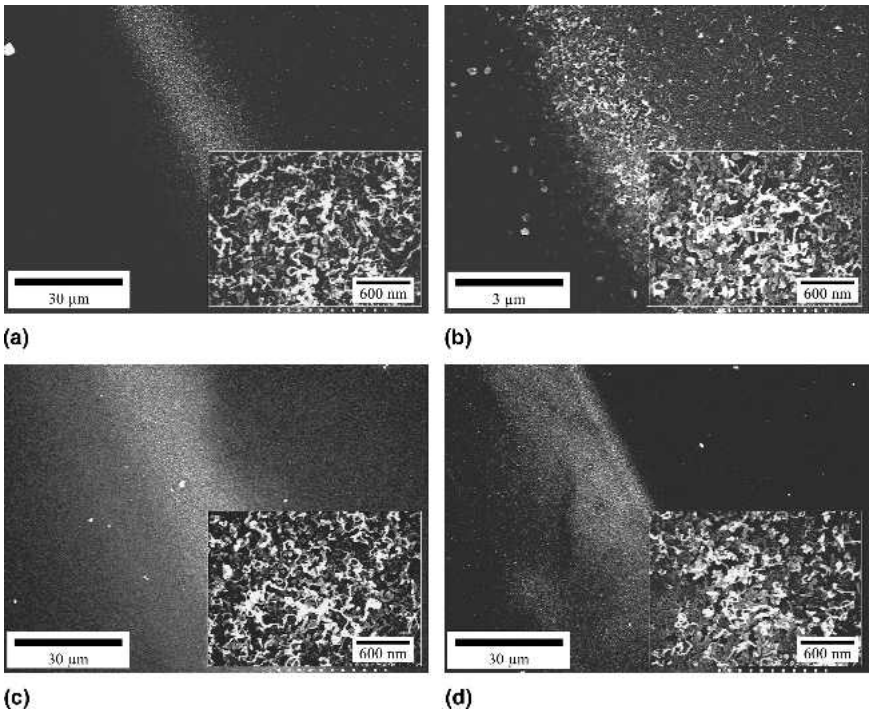

FIG. 7. Typical SEM images of the pattern boundary after TCVD by installing the fins: (a) and (b) results on the edges of point D; (c) and (d) results on point K. The images of (a) and (c) are the "shady side" and the upper-right of the image is the metal pattern. The images of (b) and (d) are the "sunny side" and the lower-left of the image is the metal pattern. The CNTs grew in the narrow region that appears as the white contrast area. The W_{CNT} was (a) 17 μm, (b) 2.6 μm, (c) 29 μm, and (d) 19 μm. The insets show magnified images.

Petitioner Runergy USA Inc., Ex. 1033, p. 2891

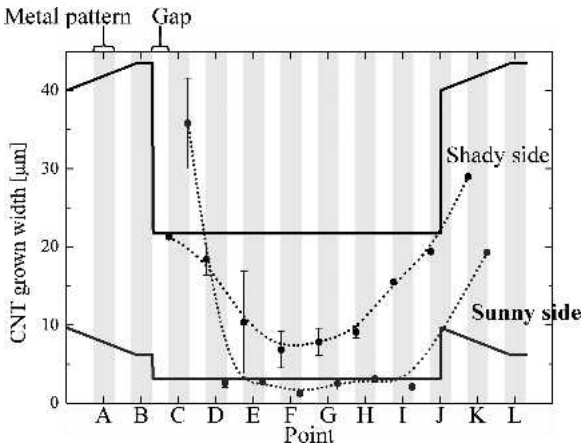

FIG. 8. The W_{CNT} observed at each point in every pattern prepared. The gray belts correspond to the metal mask patterns; white belts correspond to the pattern gaps. The solid lines show the effective width, W_{SE}.

sunny sides were narrower than those of shady sides because the number of atoms that originate from shaded directions under the edges of the mask is reduced by the fins. The W_{CNT} of shady sides depended on the position of the patterns, whereas the calculated W_{SE} was uniform between Point C and I. Figure 6(b) shows that this uniformity was attributable to the nonuniform thickness of the metal pattern. By increasing the thickness of the metal patterns, the W_{CNT} decreased, as discussed above. The thickness distribution resulted from installation of the fins. The W_{SE} and the W_{CNT} increased just under the tail of fins (Points A, B, J, K, and L) because of increased incident angles. The sputtered atoms were deposited through the left and right sides of the fin. Because the W_{SE} contains not only thin and rough regions, but also thick and smooth regions, the W_{SE} was larger than the W_{CNT}.

An electric field was applied during CVD to obtain VACNTs. Figure 9 shows SEM images of CNTs grown using TCVD only, applying a bias without a glow discharge [Fig. 9(a)], and PECVD with a glow discharge accompanying the discharge current [Fig. 9(b)]. The CNTs with an approximate 15-nm diameter grew in various, apparently random, directions using the TCVD method. The CNTs grew selectively near the boundary of the metal pattern. Effects of the applied bias during TCVD were not observed. In the case of PECVD method, CNTs with an approximate 25-nm diameter grew perpendicular to the surfaces. The VACNTs were observed throughout the pattern. Figure 10 shows a TEM image of CNTs grown using PECVD. The hollow center and graphitic sidewalls were observed. In this case, the number of walls was 25, and the CNT internal and external diameters were approximately 4.6 and 26 nm, respectively.

The VACNTs were achieved only through the use of

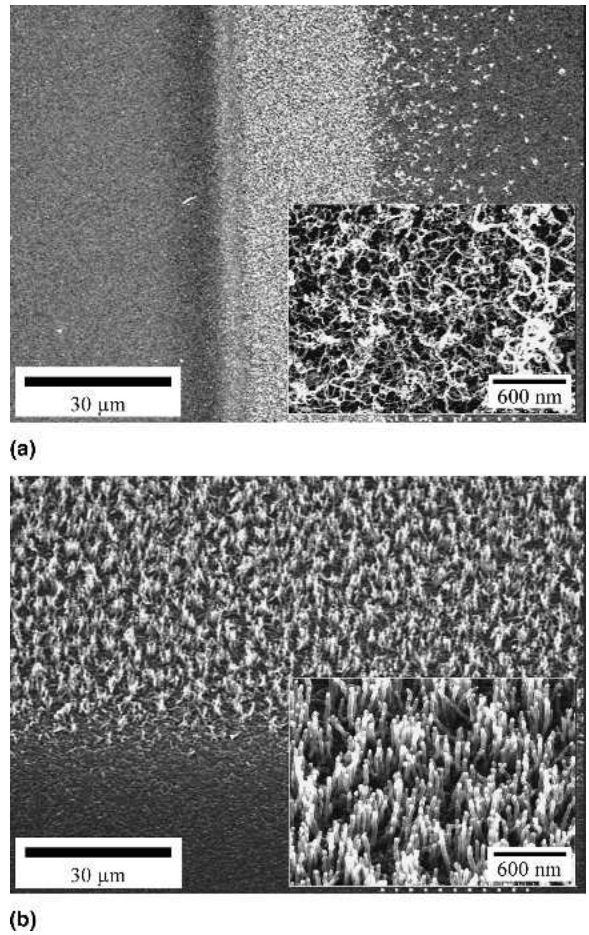

FIG. 9. SEM images of CNTs grown using TCVD only (a) applying bias without a discharge and (b) PECVD with a glow discharge. An applied bias voltage was −300 V [(a) discharge current of approximately 0.005 A]; and −250 V [(b) discharge current of approximately 0.3 A]. Images of (b) were taken at a 45° tilt angle. The inset shows magnified images.

PECVD method. The voltage drop takes place mostly in the cathode dark space when a glow discharge is induced. The thickness of the cathode dark space was estimated using the Child-Langmuir law. The estimated thickness of the cathode dark space was 0.21 mm. Then, the electric field induced above the substrates was approximately 1.2 kV/mm^{-1}. The cathode dark space thickness was estimated in the case of TCVD also. The estimated cathode dark space thickness was 60 mm, which was larger than the distance separating the cathode and anode. Therefore, the electric field might be uniform in the space between the cathode and the anode. The electric field above the substrates was approximately 60 V/mm^{-1}. The electric field applied in the case of PECVD was approximately 20 times larger than that in TCVD. The CNTs grew throughout the pattern by PECVD, whereas selective growth was observed using TCVD. This result suggests that the Ni catalysts were changed into fine particles by bombardment of ions accelerated in a large electric field.

Petitioner Runergy USA Inc., Ex. 1033, p. 2892

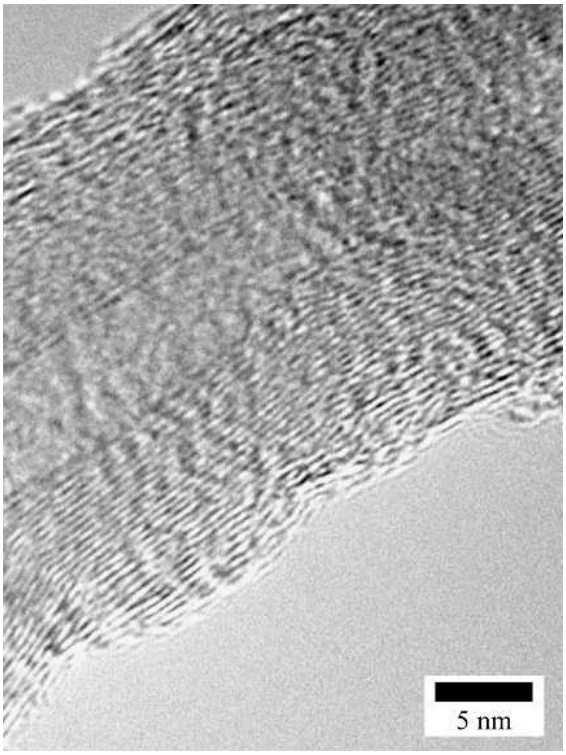

FIG. 10. Typical TEM image of CNTs grown using PECVD.

Results showed that CNTs were able to grow even on the smooth metal patterns.

IV. CONCLUSIONS

We prepared CNTs and VACNTs grown selectively on patterned metal. The selectively grown CNTs were observed at the edges of the patterned metal using TCVD. By controlling not only the catalyst position, but also the surface morphology of their underlayers, the width of selectively grown CNTs was minimized to approximately 2.6 μm. That width was approximately one-eightieth that of the patterned metal, which was 200 μm. To prepare VACNTs, DC-negative bias voltage was applied to the substrates. The VACNTs were synthesized when the glow discharge took place in the PECVD. The VACNTs grew all over the patterned metal. Selective growth of CNTs was achieved in optimum conditions of the TCVD by controlling the morphology of the Mo underlayers for Ni catalysts.

ACKNOWLEDGMENTS

This work was supported by a Grant-in-Aid from the Futaba Foundation. This work was also supported by a Ministry of Education, Culture, Sports, Science and Technology through a Scientific Grant-In-Aid (No. 15360173).

REFERENCES

1. J. Kong, E. Yenilmez, T.W. Tombler, W. Kim, H. Dai, R.B. Laughlin, L. Liu, C.S. Jayanthi, and S.Y. Wu: Quantum interference and ballistic transmission in nanotube electron waveguides. *Phys. Rev. Lett.* **87,** 106801 (2001).
2. Z. Yao, C.L. Kane, and C. Dekker: High-field electrical transport in single-wall carbon nanotubes. *Phys. Rev. Lett.* **84,** 2941 (2000).
3. E.W. Wong, P.E. Sheehan, and C.M. Lieber: Nanobeam mechanics: Elasticity, strength, and toughness of nanorods and nanotubes. *Science* **277,** 1971 (1997).
4. J.H. Hafner, C.L. Cheung, and C.M. Lieber: Growth of nanotubes for probe microscopy tips. *Nature* **398,** 761 (1999).
5. R. Stevens, C. Nguyen, A. Cassell, L. Delzeit, M. Meyyappan, and J. Han: Improved fabrication approach for carbon nanotube probe devices. *Appl. Phys. Lett.* **77,** 3453 (2000).
6. T. Arie, H. Nishijima, S. Akita, and Y. Nakayama: Carbon-nanotube probe equipped magnetic force microscope. *J. Vac. Sci. Technol., B* **18,** 104 (2000).
7. S. Fan, M.G. Chapline, N.R. Franklin, T.W. Tombler, A.M. Cassell, and H. Dai: Self-oriented regular arrays of carbon nanotubes and their field-emission properties. *Science* **283,** 512 (1999).
8. N. Saurakhiya, Y.W. Zhu, F.C. Cheong, C.K. Ong, A.T.S. Wee, J.Y. Lin, and C.H. Sow: Pulsed laser deposition-assisted patterning of aligned carbon nanotubes modified by focused laser beam for efficient field emission. *Carbon* **43,** 2128 (2005).
9. W.I. Milne, K.B.K. Teo, G.A.J. Amaratunga, R. Lacerda, P. Legagneux, G. Pirio, V. Semet, and V.T. Binh: Aligned carbon nanotubes/fibers for applications in vacuum microwave devices. *Curr. Appl. Phys.* **4,** 513 (2004).
10. A.C. Dupuis: The catalyst in the CCVD of carbon nanotubes—a review. *Prog. Mater. Sci.* **50,** 929 (2005).
11. V.I. Merkulov, A.V. Melechko, M.A. Guillorn, D.H. Lowndes, and M.L. Simpson: Alignment mechanism of carbon nanofibers produced by plasma-enhanced chemical-vapor deposition. *Appl. Phys. Lett.* **79,** 2970 (2001).
12. L. Delzeit, B. Chen, A. Cassell, R. Stevens, C. Nguyen, and M. Meyyappan: Multilayered metal catalysts for controlling the density of single-walled carbon nanotube growth. *Chem. Phys. Lett.* **348,** 368 (2001).

Petitioner Runergy USA Inc., Ex. 1033, p. 2893